40th AIAA/ASME/SAE/ASEE Joint Propulsion Conference and Exhibit
11-14 July 2004, Fort Lauderdale, Florida

AIAA 2004-3954

Particle Simulation of Plasma Dynamics Inside an Anode-Layer Hall Thruster

Kimiya KOMURASAKI, Shigeru YOKOTA,† Shinsuke YASUI,† and Yoshihiro ARAKAWA‡*
The University of Tokyo, Hongo 7-3-1, Bunkyo, Tokyo 113-8656, JAPAN

Keywords: Electric Propulsion, Hall Thruster, Hollow Anode、PIC-DSMC Method

Abstract

Plasma dynamics inside a discharge channel including a cavity of a hollow anode was numerically analyzed using fully kinetic 2D3V Particle-in-Cell (PIC) and Direct Simulation Monte Carlo (DSMC) methods. The results reproduced both stable and unstable operation modes observed in the experiment using a 1kW-class anode layer type hall thruster. In the stable operation case, which corresponds to the case with low magnetic flux density, the plasma penetrated into the hollow anode deeply. This suggests that comparably large substantial anode area should contribute to stable operation.

INTRODUCTION

Discharge instability in anode layer hall thrusters would be one of the serious problems to be overcome. A hollow anode is commonly used to stabilize the discharge for these thrusters.[1-3] However, the mechanism of discharge stabilization using a hollow anode has not been clarified yet and optimization of anode design has not been done.

The goal of our study is to model the anode sheath, which has a great effect on the stable discharge of anode layer hall thrusters, and find out a scaling law for the anode design.

In the computational study, the structure of electrical sheath inside a hollow anode was numerically simulated using fully kinetic 2D3V Particle-in-Cell (PIC) and Direct Simulation Monte Carlo (DSMC) methodologies.[4-9] The results are compared with the measurement using a 1-kW class anode layer hall thruster.

DISCHARGE INSTABILITY

A 1kW-class anode layer hall thruster with a hollow anode has been designed and fabricated in the university of Tokyo. It has two guard rings made of stainless steel. They are kept at the cathode potential. The inner and outer diameters of a discharge chamber are 48mm and 62mm, respectively. Magnetic flux density is variable by changing the current of a solenoid coil set at the center of the thruster. Detailed description is available in Refs. 3,4).

* Associate Professor, Department of Advanced Energy, Member AIAA, komurasaki@k.u-tokyo.ac.jp
† Graduate Student, Department of Aeronautics and Astronautics
‡ Professor, Department of Aeronautics and Astronautics, Member AIAA

It has an annular hollow anode made of cupper. We define Z as the distance between the thruster exit and the tip of anode, and D as the width of propellant channel as indicated in Fig. 1. Z and D are varied (Z=1~4mm, D=1~3mm) in this study. Xenon is used as a propellant, and the mass flow rate is set at $1.0A_{eq}$=1.37mg/s. Discharge voltage is set at 400V.

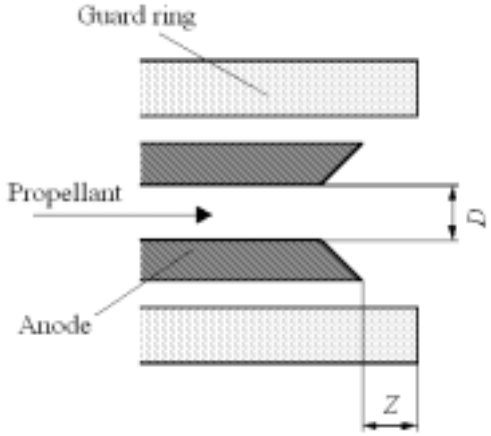

Fig. 1 Definitions of the geometric parameters *Z* and *D*.

The measured dischrge current histories are shown in Fig. 2. Figure 3 shows measured amplitude of discharge current oscillation and the time-averaged discharge current $\overline{I_d}$. Here, the amplitude of discharge current oscillation is defined as,

$$\Delta = \sqrt{\int_0^\tau (I_d/\overline{I_d} - 1)^2 dt \Big/ \tau} \qquad (1)$$

Oscillation amplitude was sensitive to magnetic flux density B. Although the oscillation is small at B<0.014T, the thrust efficiency is poor in this range of B because of large electron backflow current. Therefore, the desirable operation condition is limited in a quite narrow range of B.

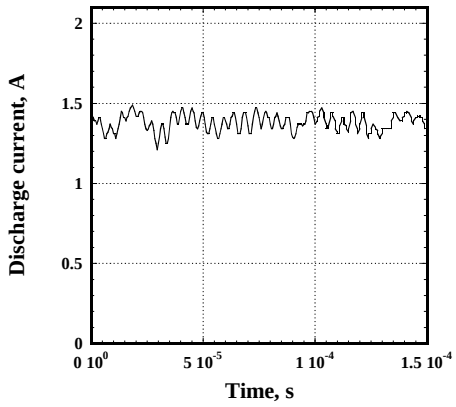

(a) *B*=0.01T

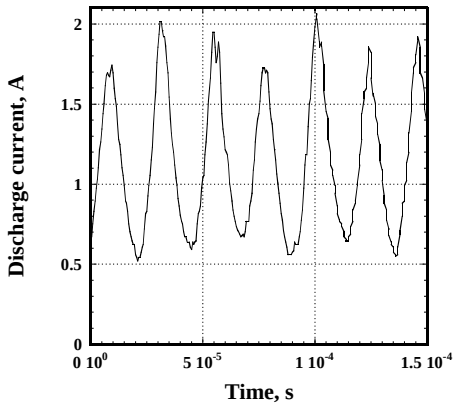

(b) *B*=0.02T

Fig. 2 Measured discharge current history. *D*=3mm, *Z*=1mm. [4)]

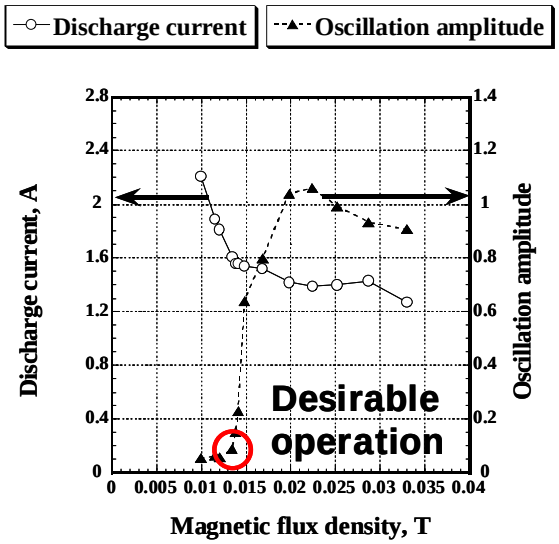

Fig. 3 Oscillation characteristics. *D*=3mm, *Z*=1mm. [4)]

Measured oscillation amplitude is plotted for various anode geometries in Fig. 4. There is a common trend that oscillation becomes unstable with the increase in *B* as seen in Fig. 3. The threshold of *B* is about 0.011-0.015[T].

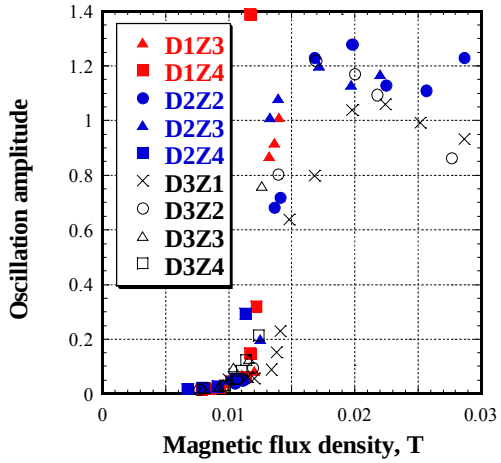

Fig. 4 Relation between oscillation amplitude and *B*. *Z*=1–4mm, *D*=1–3mm, V_d=400V. [4)]

CALCULATION METHOD

Computational Methods and Physical Models

It is very difficult to measure the distributions of electric potential and plasma density inside a hollow anode because plasma density is expected very small and the plasma is electrically non-neutral. Therefore, structure of electrical sheath inside the hollow anode and plasma dynamics in the discharge channel were numerically computed using fully kinetic 2D3V Particle-in-Cell (PIC) and Direct Simulation Monte Carlo (DSMC) methodologies. By treating both electrons and ions as a particle, non-neutral plasma structure in the sheath region near the anode surface can be analyzed. Figure 5 shows the flow chart of calculation.

10^6-10^9 of real particles are treated as one macro particle and all of macro particles are treated kinetically. Electric and magnetic forces are implemented via the PIC method and collisions are via the DSMC method. The cylindrical coordinate system (r, z, θ) was used as shown in Fig. 6. Particle's position is expressed in two-dimensional space r and z, while its velocity is expressed in three-dimensional space. That is, particles move in all directions, but the azimuthal coordinate is always discarded.

An orthogonal calculation grid is set, with the axial length of the cell getting smaller toward the discharge channel in order to observe the sharp fall of electron density in the vicinity of anode exit. The minimum cell length is in the same order of the Debye length.

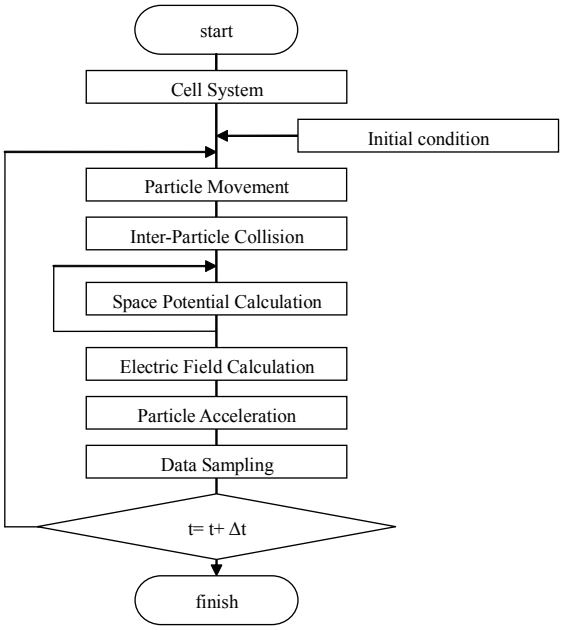

Fig. 5 A flow chart of the calculation.

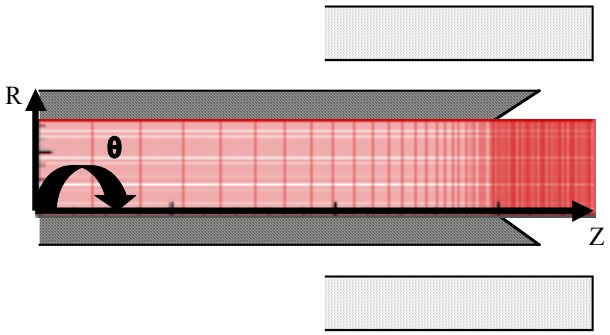

Fig. 6 The coordinate and the calculation grid.

Assumptions for this computation are listed below:

- Magnetic field lines are aligned in the radial direction and don't have axial or azimuthal components. Figure 7 shows the assumed magnetic flux density distribution in the calculation. B_0 is variable.
- Only singly charged ionization is considered.
- Mass ratio m_e/m_n is decreased from 4×10^{-6} to 1/100, to speed up the calculation.
- Potential difference between anode and plasma at the thruster exit boundary is set at 250V.

Propellant mass flow rate is set at $1.0A_{eq}$ to simulate the experiment. Electrons are fed from the anode exit with a T_e=10eV half-Maxwellian velocity distribution.

Collisions considered in this simulation are shown in Table 1. The mean free time and collision frequency ν in the table are typical values when the particles are at their thermal velocity. The simulation time step (typically 1.22×10^{-11}s) is set based on Larmor frequency, and that is much smaller than e^-–Xe collision mean free time.

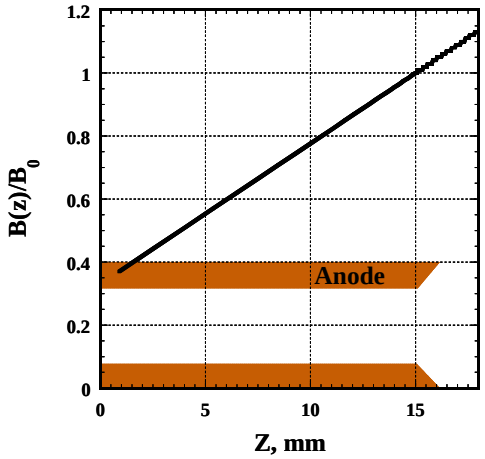

Fig. 7 Assumed magnetic flux density distribution.

Table 1 Collisions considered in the simulation and their typical collision frequency ν.

Collision	Mean Free Time, ps	Relative ν
e^-–Xe Elastic Scattering	2.038	1.00
e^-–Xe Ionization	18.31	0.111
e^-–Xe Excitation	66.83	3.05×10^{-2}
e^-–Xe^+ Coulomb	282.7	7.21×10^{-3}
e^-–e^- Coulomb	15270	1.33×10^{-4}
Xe – Xe Scattering	38300	5.32×10^{-5}

All the particles move according to the dynamic equations. The dynamic equations for electrons are expressed as,

$$m_e\ddot{z} = -e(E_z - r\dot{\theta}B_r) \quad , \qquad (1)$$

$$m_e\ddot{r} = -eE_r + m_e r\dot{\theta}^2 \, , \qquad (2)$$

$$m_e r\ddot{\theta} = -e\dot{z}B_r - m_e\dot{r}\dot{\theta} \quad . \qquad (3)$$

and for ions,

$$m_i\ddot{z} = eE_z \quad , \qquad (4)$$

$$m_i\ddot{r} = eE_r \quad . \qquad (5)$$

Space potential ϕ is calculated using the Poisson's equation as,

$$\frac{\partial^2\phi}{\partial z^2} + \frac{1}{r}\frac{\partial}{\partial r}\left(r\frac{\partial\phi}{\partial r}\right) = -\frac{e}{\varepsilon_0}(n_i - n_e) \, . \qquad (6)$$

RESULTS AND DISCUSSIONS

Figure 8 shows the calculated discharge current histories. In the case of B_0=0.01T, discharge is stable. Discharge current is 1.3A and oscillation amplitude is 0.01. The discharge current level is well agreed with the measurement.

On the other hand, in the case of B_0=0.015T, strong discharge oscillation was observed. Oscillation frequency(～60kHz) is very close to the measured one (～50kHz.) Averaged discharge current is 0.8A

In the case of B_0=0.02T, averaged discharge

current is 0.3A, which is smaller than the measured one. This would be because the electron backflow mechanism has transited from classical diffusion to Bohm diffusion in the experiment. In this computation model, Bohm diffusion has not been implemented yet. (Disturbance in the azimuthal direction has been discarded.)

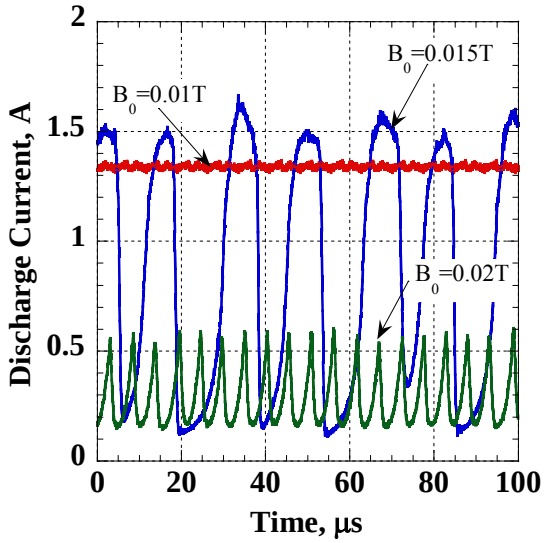

Fig. 8 Computed discharge current history. *Z*=3mm, *D*=3mm.

Figure 9 shows the computed discharge current oscillation amplitude. The amplitude was high at $B_0 \geqq 0.015$T. This trend agrees well with the measured one as seen in Figs. 3 and 4.

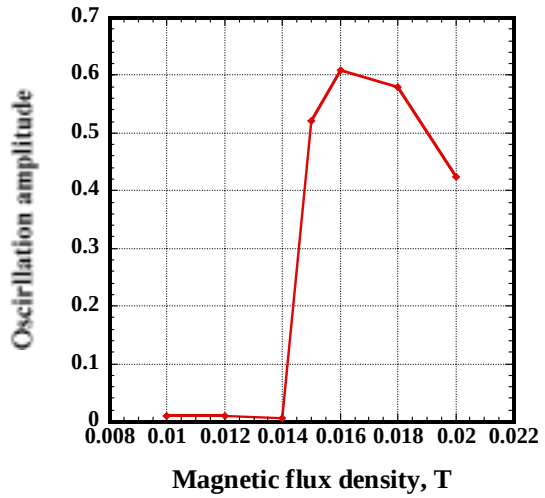

Fig. 9 Computed discharge current oscillation amplitude.

Calculated two-dimensional distributions of electron number density are shown in Fig. 10. In the case of $B_0 \leqq 0.014$T (Fig.10 (a) and (b)) the distributions are stable. For B_0=0.010T, magnetic confinement against the electron backflow is not enough and large electron current flows in the discharge channel. In the case of B_0=0.014T, electron is trapped by the magnetic field, and density peaks in the middle of discharge channel. Plasma has penetrated into the anode cavity resulting in large substantial anode surface area that contacts the plasma. Then, electrons would be able to reach the anode smoothly without a large sheath drop. The ionization reaction inside the hollow anode contributes to this profile. The fraction of propellant gas that is ionized in the hollow anode is about 30%.

In the case of $B_0 \geqq 0.015$T (Fig.10 (c) and (d)) the discharge is oscillating. The island of high-density electrons seen inside the hollow anode is moving back and forth in the z-direction. Although the gas is ionized inside the hollow anode, the density distribution is discontinuous and ionization instability has seen observed.

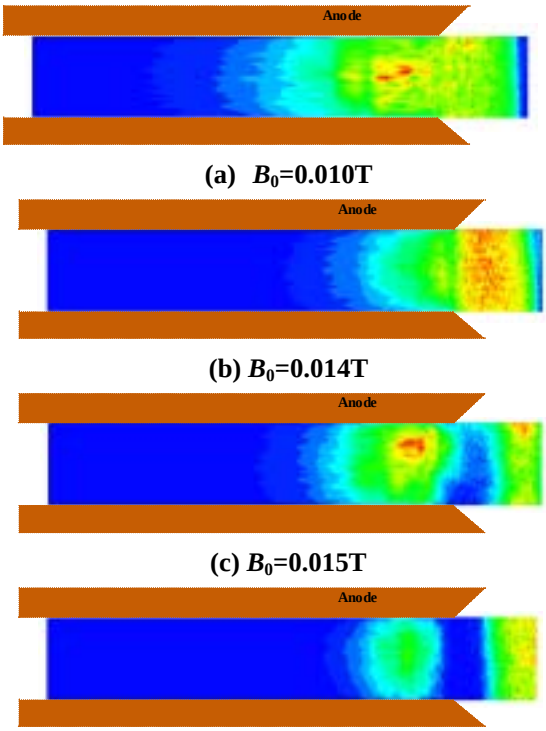

(a) B_0=0.010T

(b) B_0=0.014T

(c) B_0=0.015T

(d) B_0=0.020T

Fig. 10 Computed electron number density distributions. Contour max 2.0×10^{18}m^{-3}, min 0.2×10^{18}m^{-3}. (a) and (b) are steady solutions. (c) and (d) are snapshots of oscillating profiles.

Figure 11 shows electron current density distribution on the anode surface. The anode length effective for electron current is about 10mm for *D*=3mm. Figure 12 shows the computed plasma potential distributions. In the case of $B_0 \leqq 0.014$T, a potential drop appears at the exit of discharge channel. This corresponds to the potential variation outside the exit as seen in the measured potential profiles. (Fig. 13) The plasma potential is linearly varied though the anode exit

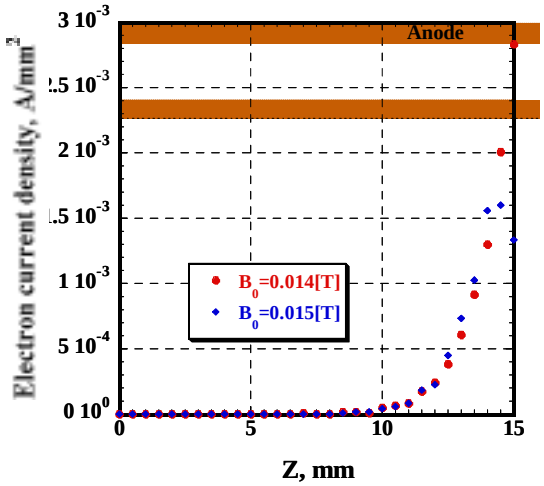

Fig. 11 Discharge current distribution on the anode surface.

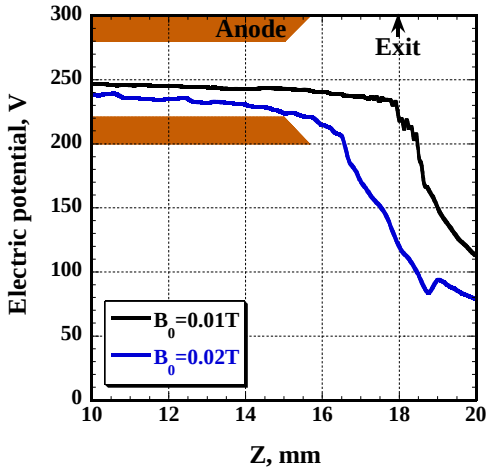

Fig. 13 Electric potential measured in experiment. Discharge voltage was 250V.[3)]

In the case of $B_0 \geqq 0.015$T, potential starts to decrease at the anode exit. This tendency is same as the measured potential profiles as well. (Fig. 13) This rapid potential decrease at the anode exit is identical to the one without an anode hollow. The electron density tends to be small due to the rapid acceleration by the electric field resulting in shortage of plasma density on the anode surface.

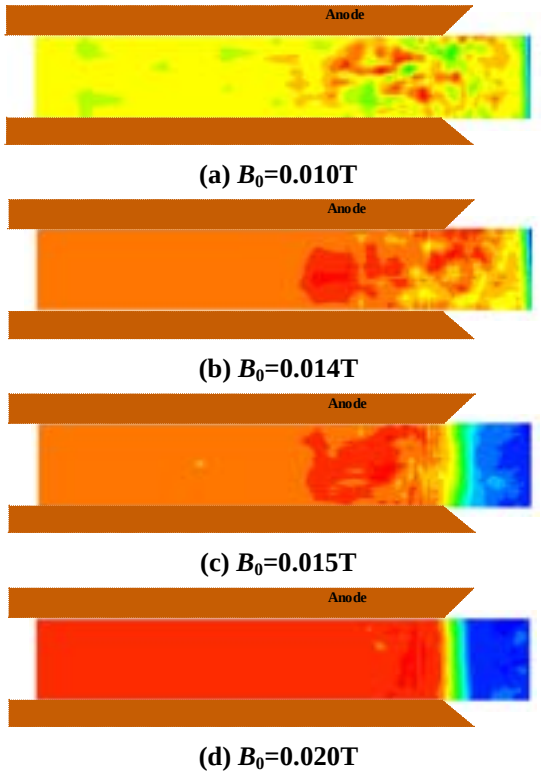

Fig. 12 Computed plasma potential distributions. Contour max 250V, min 0V. (a) and (b) are steady solutions. (c) and (d) are snapshots of oscillating profiles.

Figure 14 shows the computed electron temperature distributions. In the case of $B_0 \geqq 0.015$T, high temperature region is limited in a thin layer located at the exit of anode. This is due to the strong electric field as seen in Fig. 12. This rapid increase in temperature contributes to the high ionization rate inside the hollow anode, and brings the ionization oscillation inside the hollow anode. To suppress the ionization oscillation, linear variation in plasma potential though the anode exit would be necessary.

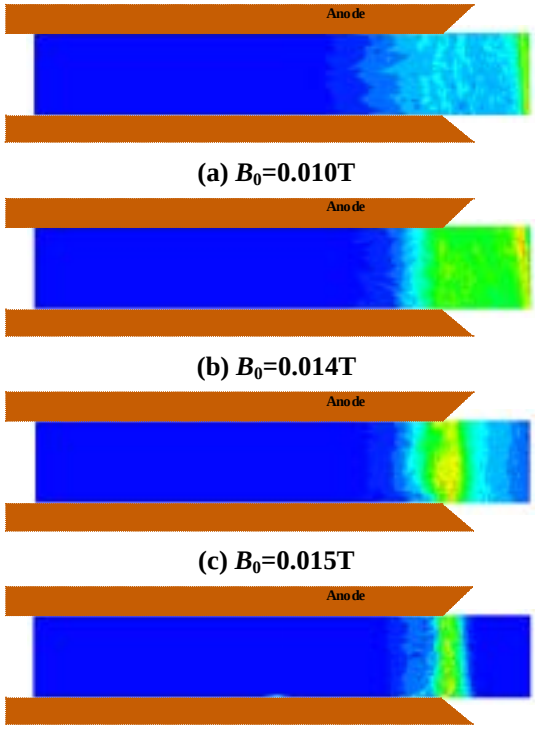

Fig. 14 Computed electron temperature distributions. Contour max 100eV, min 0eV. (a) and (b) are steady solutions. (c) and (d) are snapshots of oscillating profiles.

As seen in Figs. 12-14, ionization and acceleration occurs in a thin layer at the anode exit in the high magnetic flux density cases. This is a typical feature of anode layer type or sheath type thruster.

The condition in which the layer appears will be a function of operating and geometric parameters of the thruster. Then, optimization of the hollow anode geometry for typical operational condition would be one way to suppress the oscillation. Another way would be to have a discharge independent of the main discharge to assist the ionization in the hollow anode.

CONCLUSION

The fully kinetic PIC-DSMC code can reproduce both stable and unstable operation modes observed in the experiment.

In the stable operation case, which corresponds to the low magnetic flux density case, the plasma penetrated into the anode cavity. This large substantial anode area would contribute to stable operation.

In the unstable operation case, which corresponds to the high magnetic flux density case, ionization oscillation was observed inside the hollow anode. This would be caused by the non-linear variation of plasma potential at the anode exit.

To suppress the ionization oscillation, linear variation in plasma potential though the anode exit would be necessary.

REFERENCES

1) Semenkin A.V., Tverdokhlebov S.O., Garkusha V.I., Kochergin A.V., Chislov G.O., Shumkin B.V., Solodukhin A.V., Zakharenkov L.E., "Operating Envelopes of Thrusters with Anode Layer", IEPC2001-013, 27th International Electric Propulsion Conference, Pasadena, USA, October 2001.
2) Semenkin, A., Kochergin, A., Garkusha, V., Chislov, G., Rusakov, A., "RHETT/EPDM Flight Anode Layer Thruster Development", IEPC-97-106, 25th International Electric Propulsion Conference, Cleveland, USA, August 1997.
3) Yamamoto, N., Nakagawa, T., Komurasaki, K., Arakawa, Y., "Effect of Discharge Oscillations on Hall Thruster Performance", ISTS 2002-b-17, 23rd the International Symposium on Space Technology and Science, Shimane, Japan, May 2002.
4) Yasui, S., Yamamoto, N., Komurasaki, K., Arakawa, Y., "Effect of Sheath Structure on Operating Stability in an Anode Layer Thruster," Proceedings of Asian Joint Conferences in Propulsion and Power 2004, pp.382-387, Seoul, Korea, March 2004.
5) Hirakawa, M., "Particle Simulation of Plasma Phenomena in Hall Thrusters", IEPC-95-164, 24th International Electric Propulsion Conference, Moscow, Russia, September 1995..
6) Szabo, J. J., "Fully Kinetic Hall Thruster Modeling of a Plasma Thruster", PhD Thesis, Massachusetts Institute of Technology, 2001.
7) Szabo, J., Rostler, P., "One and Two Dimensional Modeling of the BHT-1000", IEPC-02-231, 28th International Electric Propulsion Conference, Toulouse, France, March 2003.
8) Kumakura, K., Yasui, S., Komurasaki K., Arakawa, Y., "Plasma Modeling of a Hollow Anode for an Anode Layer Type Hall Thruster" IEPC-02-086, 28th International Electric Propulsion Conference, Toulouse, France, March 2003.

APPENDIX

Nomenclature

B: magnetic flux density
D: anode hollow width
e: electronic charge
E: electric field strength
I_d: discharge current
m: particle mass
n: number density
t: time
V_d: discharge voltage
x: position
Z: distance between anode tip and channel exit
ε_0: free space permeability
ϕ: space potential
ν: collision frequency
r, z, θ: cylindrical coordinate

Subscripts

0: anode exit
e: electron
i: ion
n: neutral